Spiking Neural Networks for Crop Yield Estimation Based on Spatiotemporal Analysis of Image Time Series

Pritam Bose, Nikola K. Kasabov, *Fellow, IEEE*, Lorenzo Bruzzone, *Fellow, IEEE*, and Reggio N. Hartono

***Abstract*—This paper presents spiking neural networks (SNNs) for remote sensing spatiotemporal analysis of image time series, which make use of the highly parallel and low-power-consuming neuromorphic hardware platforms possible. This paper illustrates this concept with the introduction of the first SNN computational model for crop yield estimation from normalized difference vegetation index image time series. It presents the development and testing of a methodological framework which utilizes the spatial accumulation of time series of Moderate Resolution Imaging Spectroradiometer 250-m resolution data and historical crop yield data to train an SNN to make timely prediction of crop yield. The research work also includes an analysis on the optimum number of features needed to optimize the results from our experimental data set. The proposed approach was applied to estimate the winter wheat (*Triticum aestivum L.*) yield in Shandong province, one of the main winter-wheat-growing regions of China. Our method was able to predict the yield around six weeks before harvest with a very high accuracy. Our methodology provided an average accuracy of 95.64%, with an average error of prediction of 0.236 t/ha and correlation coefficient of 0.801 based on a nine-feature model.**

***Index Terms*—Crop yield forecasting, estimation, machine learning, Moderate Resolution Imaging Spectroradiometer (MODIS), normalized difference vegetation index (NDVI), remote sensing, spiking neural networks (SNNs).**

I. Introduction

CROP production plays a vital role in food security and economic development of a country. In the past years, the fluctuation of crop yield in China attracted a great concern in economy and even led to food crisis of the whole country. For example, a continuous drought in Yunnan Province in 2011 caused approximately 340 million U.S. dollar loss because of the substantial crop yield reduction and further resulted in significant price increases [1].

Application of remote sensing data to agriculture and crop production has been popular, especially based on the predictive empirical models, because it is possible to efficiently and quantitatively estimate crop yield by such data [2]–[5]. The normalized difference vegetation index (NDVI), a product derived from satellite multispectral data, can be used to estimate the vegetation health and monitor changes in vegetation [4], [5]. It is calculated from the normalized total reflectance of the red and near infrared (NIR) bands, ranging from -1.0 to $+1.0$ [6]. A higher NDVI indicates more green coverage, whereas a lower NDVI signifies the loss of growth and vigor of the crop. Therefore, the NDVI temporal profile rises with the growth of crops and typically reaches the peak level during the productive stage, and declines around the harvest [7]. NDVI data derived from the National Oceanic and Atmospheric Administration (NOAA) Advanced Very High Resolution Radiometer (AVHRR) have been used to forecast crop yield in many countries since the 1980s. For instance, monthly global area coverage NDVI data were used to estimate cop yield in Mediterranean African countries [8]. Decadal average NDVI data were adopted to forecast corn yield in Swaziland [9]. Similar studies have been conducted for various crop types in many other regions, e.g., wheat in Morocco [10] and Italy [11], millet in Senegal [12], and corn in Kenya [13].

NDVI data from the Moderate Resolution Imaging Spectroradiometer (MODIS) available from 2000 to the present have made significant improvements addressing the shortcomings from AVHRR [14], [15]. In past years, studies have been conducted to set up the relationship between crop yield and NDVI data from MODIS. The spatial accumulative and smoothed MODIS-NDVI data were used to estimate winter wheat production in Shandong province, China [16]. MODIS data were used to establish an empirical approach to winter wheat estimation in Kansas and Ukraine [17]. Weighted NDVI temporal series from MODIS were applied to forecast sugarcane yield in Kenya [18] and using MODIS-NDVI data with an analysis of cropland mask choice and ancillary data for annual crop yield forecasting in Midwestern U.S. [19].

The NDVI information is data intensive and correlates nonlinearly with spatial-based crop yield. Therefore, a proper model building technique for crop yield prediction is essential. A general method previously used by researchers was based on statistical model building [20]–[22]. Black [23] suggested that

Manuscript received February 12, 2016; revised June 3, 2016; accepted June 24, 2016. Date of publication July 28, 2016; date of current version September 27, 2016. This work was supported by the Auckland University of Technology SRIF Grant to KEDRI and by the exchange collaboration agreement between AUT and University of Trento.

P. Bose is with the Department of Information Engineering and Computer Science, University of Trento, 38123 Trento, Italy (e-mail: pritam.bose@alumni.unitn.it).

N. K. Kasabov and R. N. Hartono are with the Knowledge Engineering and Discovery Research Institute, Auckland University of Technology, Auckland, 1010, New Zealand (e-mail: nkasabov@aut.ac.nz; reggionh@gmail.com).

L. Bruzzone is with the Remote Sensing Laboratory, Department of Information Engineering and Computer Science University of Trento, 38123 Trento, Italy (e-mail: lorenzo.bruzzone@unitn.it).

Color versions of one or more of the figures in this paper are available online at http://ieeexplore.ieee.org.

Digital Object Identifier 10.1109/TGRS.2016.2586602

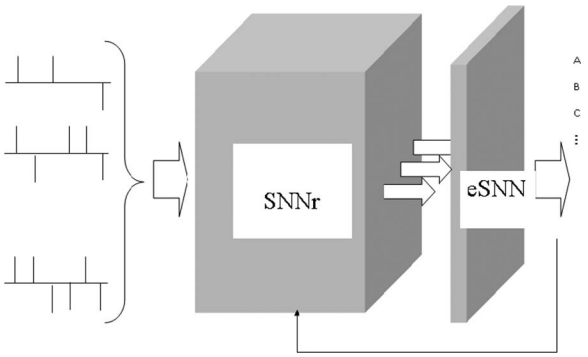

Fig. 1. General architecture of the NeuCube. Spike trains, which represent continuous value data from the input data stream, are fed to an SNNr, and the neuron firing state vectors of this reservoir are used to train an output classifier/regressor [37], [44], [45].

Fig. 2. Location of the study region.

the complexity of the total environment affects crop production. Considering the nature of the data used for crop yield modeling, neural network (NN) modeling techniques can be a solution to the estimation problem. NNs have the ability of computing, processing, predicting, and classifying data. This approach has the advantages of nonlinearity, input–output mapping, adaptivity, generalization, and fault tolerance [24]. An NN can be seen as a massive parallel-distributed processor that has the natural capability of storing experimental knowledge and making it available through generalization for use in prediction. Through learning procedures, artificial NNs (ANNs) can approximate any nonlinear relationship that exists between a set of inputs and their corresponding set of outputs [25]. Zhuang and Engel, and Ranaweera *et al.* [26], [27] provided evidence regarding the advantages of NN modeling techniques over the statistical process in the case of nonlinear data modeling, to diminish collinearity problems and model flexibility.

The approach that we present in this paper is based on the third generation of ANNs, which are called spiking NNs (SNN). SNNs have been shown to outperform the aforementioned traditional methods in many data processing tasks [28]–[36]. Spatiotemporal pattern recognition in remote sensing is a complex problem, and the most commonly used models for dealing with temporal information, based on hidden Markov models and traditional ANNs, have a limited capacity to achieve the integration of complex and long temporal spatial/spectral components because they usually either ignore the temporal dimension or oversimplify its representation [37]. SNN explicitly encodes temporal information by transforming input data into trains of spikes that represent time-sensitive events. Several variants of SNN, namely, evolving SNN (eSNN) [38]–[40] and dynamic eSNN (deSNN) [41]–[43], have been proposed in the pattern recognition literature. Recently, a new SNN computational architecture has been proposed, called NeuCube [45]. NeuCube was initially designed to process streams of spatiotemporal brain data at the timescale of milliseconds. Here, we introduce and adapt the use of this technique in remote sensing for modeling of image time series (in our case for prediction of crop yield) and for an early prediction of events.

The key components of the proposed methodology and of the NeuCube toolset are shown in Fig. 1. It shows that continuous value input data are transformed into trains of positive and negative spikes (binary units) which are then fed into a learning 3-D SNN reservoir (SNNr) before being sent to an output classifier/regressor (e.g., eSNN and deSNN) which maps SNNr states into a set of predefined output classes or predictive output values. Transforming continuous value input data into spike trains can be achieved in several ways. The one that we will explore is called address event representation (AER), where positive changes of the input data that are above a threshold generate positive spikes and negative changes lead to negative spikes [44], [45].

Learning in the SNNr can be done in one pass of data propagation [37], [44], [45] which is on large data sets and also for incremental adaptation of the learned model based on new data made continuously available. This characteristic of an SNNr has been trialed in the NeuCube toolset in a number of studies [44]–[46], and it was shown to outperform traditional machine learning classifiers on spatiotemporal and spectrotemporal brain data. We expect the proposed method to manifest these features on spatiotemporal remote sensing satellite data streams and to become a general method and toolset for this class of problems. The objective of this paper is to develop and evaluate our SNN model for predicting crop yield using NDVI information. The main novel contributions of this paper are the following: 1) to introduce and adapt to remote sensing the SNNs for the spatiotemporal analysis of image time series; 2) to exploit the properties of SNNs to predict crop yield by using time series of MODIS images; and 3) to validate the proposed approach on a study area in Shandong province, China. This paper is organized in five sections. Section II introduces the considered study area and the used remote sensing data sets. Section III presents the proposed SNN model and architecture. Section IV illustrates the experimental results. Finally, Section V draws the conclusion of this paper.

II. Data and Methods

A. Study Area

Our study area is Shandong province, which is a part of Huanghauaihai Plain which is shown in Fig. 2. The study area includes 11 counties, which cover about 1.20×10^4 km^2. Huanghauaihai Plain is in Northern China, extending northward

TABLE I
ANNUAL YIELD, PLANTING ACREAGE, AND YIELD PER HECTARE OVER A 14-YEAR PERIOD FROM 2000 TO 2013 FOR THE CONSIDERED TEST SITE

YEAR	2000	2001	2002	2003	2004	2005	2006
Annual Yeild In (1000 tons)	1859.92	1655.15	1546.92	1564.8	1575.2	1798.4	2012.82
Planting Acreage In (1000 ha)	374.78	354.57	339.71	310.46	293.7	327.39	355.59
Yeild in tons per hectare	4.9626	4.6679	4.5535	5.0402	5.3632	5.4930	5.6604

YEAR	2007	2008	2009	2010	2011	2012	2013
Annual Yeild In (1000 tons)	1995.41	2034.09	2047.22	2058.57	2103.91	2179.5	2190.1
Planting Acreage In (1000 ha)	351.87	352.5	354.50	356.18	359.35	362.58	362.58
Yeild in tons per hectare	5.6707	5.7704	5.7748	5.7795	5.8547	6.0109	6.0403

from 32° to 422° N and east-west between approximately 1132° and 1202° E. This is the most important wheat-producing region. The plain includes five provinces: Hebei, Henan, Shandong, Anhui, and Jiangsu. It was formed by the alluvial deposits of the Yellow River, and it is the largest plain in China. The plain has a temperate, subhumid, and continental monsoon climate. In Shandong, it is rainy in summer and clear and dry in winter. It is milder and more humid in Shandong province than in other parts of the North China Plain. The average annual temperature in the province is between 11 °C and 14.5 °C (51.8 °F and 58.1 °F). January is the coldest month, with an average temperature between -5 °C and -1 °C. In the hottest month of July, the temperature averages between 24 °C and 27 °C (75.2 °F and 80.6 °F). Generally speaking, the temperature is lower in the east and higher in the southwest. The average annual rainfall is between 560 and 1170 mm, with most of the rain falling in summer. Winter wheat–summer maize is the dominant double cropping system on the plain [16], [47].

B. Satellite Data and Preprocessing

MODIS is a key instrument aboard the Terra and Aqua satellites, which take images of the entire Earth's surface every 1–2 days and acquire data in 36 discrete spectral bands ranging in wavelengths from 0.4 to 14.4 mm. These data have improved our understanding of global dynamics and processes occurring on land, in the oceans, and in the lower atmosphere. Contrasted with NOAA/AVHRR, MODIS has higher spatial and spectral resolutions. It also has higher spectral resolution and temporal resolution in comparison with Systeme Probatoire d'Observation de la Terre (SPOT) and thematic mapper multispectral data. Because the spectral bands of MODIS are narrow, the impact of water vapor absorption in the NIR band is minimized, the red band data are more sensitive to chlorophyll, and therefore, the quality of NDVI data is greatly enhanced [48]–[54]. As a result, MODIS-NDVI is widely used in research such as crop growth monitoring, crop yield estimation [16], crop mapping [55], vegetation phenology [56], vegetation classification [57], land use/land cover change [58], etc. In this paper, we adopted MODIS-NDVI data to estimate winter wheat yield in our study region.

The EROS MODIS (e-MODIS) NDVI data were downloaded from the U.S. Geological Survey (USGS) Earth Resources Observation and Science (EROS) Center website (http://earthexplorer.usgs.gov/). They distribute a collection of satellite-derived vegetation products generated from the MODIS. These products, known as "e-MODIS," respond to operational land monitoring applications requiring near-real-time NDVI data for comparison against historical records. Real-time and historical NDVI products are composited in ten-day intervals every five days on a geographic mapping grid. In Huanghauaihai Plain, winter wheat developed at the stage of reviving during the first ten days of March and at the stage of maturing in the first ten days of June. Considering the characteristics of winter wheat phenology and climate condition on the plain, the ten-day NDVI data from the first ten days of March to the middle ten days of April were used to predict crop yield around six weeks before harvest. Since the data were collected from the first ten days of March to the middle ten days of April for every year, we got 11 NDVI images for every year except for 2002, where we got nine images. This is due to the fact that the NDVI images for the middle ten days of March were missing from the USGS database, and we used linear interpolation technique to approximate the NDVI values for the missing days.

C. Crop Statistical Data

The crop statistical data needed in this research were production and planting acreage of winter wheat in Shandong province from 2000 to 2013. The historical yield data came from the website of the Chinese National Bureau of Statistics (http://www.stats.gov.cn/english/). The data used in this paper are given in Table I.

D. Crop Map

In order to calculate the crop NDVI value in the NDVI image correctly, image masking was used. Image masking helped

Fig. 3. Figure showing the Shandong province winter wheat crop mask (black—winter wheat cropland, white—other areas of no interest, and kms = distance in kilometers).

us to isolate the subset of a region's pixels that we were interested in rather than using all of the pixels in the scene. Generally, cropland masking and crop-specific masking are used by researchers [59]. Considering the characteristics of our study region, we decided to use the cropland masking method. In our study region, the land cover was very homogeneous, including mainly the crop of winter wheat and summer maize in one year. The growing acreage of winter wheat accounted for more than 90% of the whole arable land at all times. This characteristic of land use was decided, on the one hand, by the suitability of the natural conditions for growing winter wheat and by the cultural customs of local farmers, and, on the other hand, by the national policy guide to farmers' action of planting. Therefore, the study region was already a commodity base for grain production and one of the most important sources of national food supplies. We used the same crop mask for all of the years as shown in Fig. 3. From a visual examination, the image mask seemed to accurately depict the spatial distribution of mean wheat cultivation that appeared as concentrated in the river valleys. Even if there were changes in the growing acreage over the consecutive years, we ignored it as it was significantly small (see Table I). In our study area, we have got areas where we have winter wheat fields and areas where there are no winter wheat crop fields. Our crop mask has a pixel value of "1" for pixels corresponding to areas having winter wheat fields and "0" for other areas. The pixel value "1" is represented by dark/black pixels and "0" by white pixels (see Fig. 3). The boundary is not clear or well defined in some places of the crop mask because winter wheat fields are not placed near the geographical border of the Shandong province in all of the places. The places where the fields are present near the geographical border of the Shandong province have well-defined boundaries, and the other places do not have such well-defined boundaries.

III. Proposed SNN Model Based on the NeuCube Neuromorphic Framework

A. SNNs and the NeuCube Architecture

A single biological neuron and the associated synapses are a complex information processing machine that involves short-term information processing, long-term information storage, and evolutionary information stored as genes in the nucleus of the neuron. A spiking neuron model assumes input information represented as trains of spikes over time. When sufficient input information is accumulated in the membrane of the neuron and the neuron's postsynaptic potential exceeds a threshold, the neuron emits a spike at its axon. Some of the state-of-the-art models of a spiking neuron include the following: early models by Hodgkin and Huxley [28]; more recent models by Maas, Gerstner, Kistler, Izhikevich, and others (e.g., spike response models); integrate-and-fire model (IFM); Izhikevich models [32]; adaptive IFM; and probabilistic neurogenetic model [60].

The basic assumption underlying the implementation of most of the spiking neuron models is that it is the timing of spikes rather than the specific shape of spikes that carries neural information [31]. In mathematical terms, a sequence of the firing times—a spike train—can be described as $S(t)=\sum_f \delta(t-t^f)$, where $f=1,2,\ldots$ is the label of the spike and $\delta(\cdot)$ is a Dirac function with $\delta(t)\neq 0$ for $t=0$ and $\int_{-\infty}^{+\infty}\delta(t)dt=1$. Historically, the most common spiking neuron models are integrate-and-fire (IF) and leaky-integrate-and-fire (LIF) units [31], [61]–[63]. Both models treat biological neurons as point dynamical systems. Accordingly, the properties of biological neurons related to their spatial structure are neglected in the models. The dynamics of the LIF unit is described by the following equation:

$$C\frac{du}{dt}(t)=-\frac{1}{R}u(t)+\left(i_0(t)+\sum w_j i_j(t)\right) \tag{1}$$

where $u(t)$ is the model state variable (corresponding to the neural membrane potential), C is the membrane capacitance, R is the input resistance, $i_0(t)$ is the external current driving the neural state, $i_j(t)$ is the input current from the jth synaptic input, and w_j represents the strength of the jth synapse. For $R\to\infty$, (1) describes the IF model. In both IF and LIF models, a neuron is supposed to fire a spike at time t_f, whenever the membrane potential u reaches a certain value v called a firing threshold. Immediately after a spike, the neuron state is reset to a new value $u_{\rm res}<v$ and held at that level for the time interval representing the neural absolute refractory period.

Neurons connect and communicate with one another through specialized junctions called synapses [64], [65]. Arrival of a presynaptic spike at a synapse triggers an input signal $i(t)$ into the postsynaptic neuron. This signal corresponds to the synaptic electric current flowing into the neuron [66]. In a simple model, the time course of $i(t)$ can be described by the exponential function

$$i(t)=\int_0^\infty S_j(s-t)\exp\left(-\frac{s}{\tau_s}\right)ds \tag{2}$$

where τ_s is the synaptic time constant and $S_j(t)$ denotes a presynaptic spike train.

Given the models of neurons and synapses, we can define an SNN. Typically, an SNN is considered as a finite directed graph (V,E), with V being a set of neurons and E representing a set of synapses [67]. In particular, the set V contains a subset of input neurons $V_{\rm in}$ and a subset of output neurons $V_{\rm out}$. The firing of input neurons is assumed to be determined from outside of the SNN, which is the sets of firing times for the neurons in $V_{\rm in}$ that are given as the input of the SNN. A general

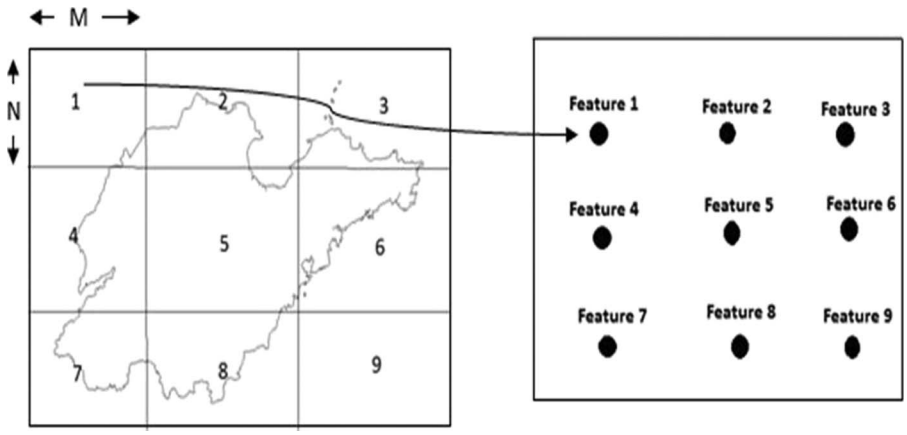

Fig. 4. Splitting of our sample space into nine equal-sized partitions of size M by N and spatial accumulation of NDVI values of each partition to form a feature.

phenomenological model describing various forms of the spike-based synaptic plasticity has been proposed by Gerstner and Kistler [68]. This model can be expressed as

$$\frac{d}{dx}w_{\mathrm{ji}}(t) = a_0 + a_1 S_i(t) + a_2 S_j(t) + a_3 S_i(t)\overline{S_j(t)} + a_4 \overline{S_i(t)} S_j(t) \quad (3)$$

where $w_{\mathrm{ji}}(t)$ is the efficacy of the synaptic coupling from neuron i to j; $S_i(t)$ and $S_j(t)$ are the pre- and postsynaptic spike trains, respectively; each spike train is defined as a sum of the Dirac impulses at the firing times t_f, i.e., $S(t) = \sum_f \delta(t - t^f)$; terms $\overline{S_i(t)}$ and $\overline{S_j(t)}$ are the low-pass-filtered versions of $S_i(t)$ and $S_j(t)$, respectively; and $a_0, \ldots, a_4$ are the constant coefficients that control the rate of change in the synaptic efficacy.

The aforementioned SNN algorithms have been implemented in the NeuCube, which is the first SNN-based spatiotemporal data machine for mapping, learning, and understanding of spatio- and spectrotemporal data [45].

B. NeuCube-Based SNN Model for Learning Spatiotemporal Patterns From Satellite Image Time Series and for Event Prediction: A Case Study of NDVI Images and Crop Volume Prediction

The NDVI images have been collected every year during the same duration from the start of March to the middle of April. The images are ten-day composite data at an interval of every five days. We have collected 11 NDVI images for each year, so over a time-span of 14 years, we have 154 MODIS-NDVI images (11 images per year *14 years). After using the image mask over the data sets, the cropped data have been extracted and stored in a comma-separated value (CSV) file for ease of use. Then, the data have been divided into equal-sized blocks and spatially accumulated NDVI values of each block acted as a feature for training of the NeuCube and future prediction (see Fig. 4). We have divided each image into equal-sized partitions, and accumulation of all of the NDVI pixel values of a region of an image is considered as a feature here. Supposing that we partition our image into n blocks, we get n features which are actually numeric values. For each year, we have 11 images, so we have $11 * n$ numeric values or features. These values are stored in individual CSV files for introducing to the SNN model. Therefore, for 14 years, we get 14 CSV files or data sets. Corresponding to each year or data set, we have statistical crop yield data. Since we multiply all of the MODIS-NDVI images with our crop mask (where the crop mask has a pixel value of "1" for pixels corresponding to areas having winter wheat fields and "0" for other areas), the values of the pixels that correspond to areas other than the winter wheat fields are considered to be "0." On partitioning the image, we get some features whose numerical value almost corresponds to 0 (see Fig. 4 in which the features obtained from block numbers 1 and 9 almost correspond to 0). These features are of no use in training since their values almost remain constant over the years, whereas the feature values change significantly in the areas that have a large number of winter wheat fields (see blocks 5 and 8 in Fig. 4). These features are highly important during the training of the SNN model. With image division, our classification algorithm was able to compare image regions rather than just global features, thus achieving better accuracy than without division. Since all regions of an image are not equally important, identifying regions of interest and analyzing those regions gave better results. During training, the NeuCube was able to identify the features that were significant and the features that were less significant in predicting the crop yield. We ran our experiments with different numbers of blocks, and we could experimentally determine the optimum number of blocks. The data encoding and training of the NeuCube were done with this processed data set and the historical winter wheat crop yield data per hectare over the time-span of 14 years.

For data encoding, there are different coding schemes in SNN, primarily rate (information as mean firing rates) or temporal (information as temporally significant) coding. For NeuCube, we use temporal coding to represent information. So far, four different spike encoding algorithms have been integrated into the existing implementation of the NeuCube, namely, the Ben's spiker algorithm (BSA), AER, step-forward spike encoding algorithm (SF), and moving-window spike encoding algorithm (MW). Different spike encoding algorithms have distinct characteristics when representing input data. BSA is suitable for high-frequency signals, and the original signal can be recovered easily from the encoded spike train because it is

based on the finite impulse response technique. Only positive (excitatory) spikes are generated by BSA, whereas all other techniques mentioned here can also generate negative (inhibitory) spikes. AER was originally implemented in hardware [69] in the artificial silicon retina. It represents significant changes in signal intensity over a given threshold, where the on and off events are dependent on the sign of the changes. However, if the changes of the signal intensity vary dramatically, it may not be possible to recover the original signal using the encoded spike train generated by AER [37]. Moreover, in our case, the data do not vary dramatically, so AER resulted in the best choice.

The spike trains, obtained after encoding the processed spatiotemporal NDVI data using the AER algorithm, were entered into the SNN cube/reservoir (SNNc; see Fig. 1) from a fixed number of corresponding brain-mapped input neurons. Mapping input variables into spatially located spiking neurons in the SNNc is a new approach toward modeling spatiotemporal remote sensing data. The main principle is that, if spatial information about the input variables is known, it can help in the following: 1) building more accurate models of the spatiotemporal data collected through these variables and 2) much better interpretation of the model and better understanding of the spatiotemporal data [37]. Since our features are spatially accumulated NDVI values, we know the location of the input variables, and we can accurately map them to spatially located spiking neurons for achieving better prediction results.

Learning in a NeuCube is a two-phase process. Learning in the SNN is first performed in an unsupervised way using spike time-dependent plasticity learning rule (STDP) [70], where spatiotemporal data are entered into relevant areas of the SNNc over time. Unsupervised learning is performed to modify the initially set connection weights. The SNNr will learn to activate same groups of spiking neurons when similar input stimuli are presented, also known as a polychronization effect [32]. Finally, with supervised training of the spiking neurons in the output module, the same data that were used for unsupervised training are now propagated again through the trained SNN, and the output neurons are trained to classify the spatiotemporal spiking pattern of the SNNc into predefined output spike sequences.

MODIS started working from 2000, so we could have NDVI satellite images only from 2000. Accordingly, the volume of data was relatively small. We used leave-one-out cross-validation technique [71] for training and testing of our model. We have 14 years of statistical crop yield data, and we need to predict these 14 years of crop yield to test the accuracy of our model. We trained our model using 13 years of data and predicted the crop yield for the remaining 1 year. We then continued the process for 14 times to predict the crop yield of 14 years. The model is repeatedly refit, leaving out a single observation, and then used to derive a prediction for the left-out observation. Therefore, the technique provided us the estimated crop yield for all of the 14 years, and we could make the comparative analysis of our results with the historical crop yield data for the 14 years to get the relative errors. Since the leave-one-out cross-validation technique might overestimate the accuracy, we also used for further confirmation of the results threefold and fivefold cross-validation techniques for training and testing our model.

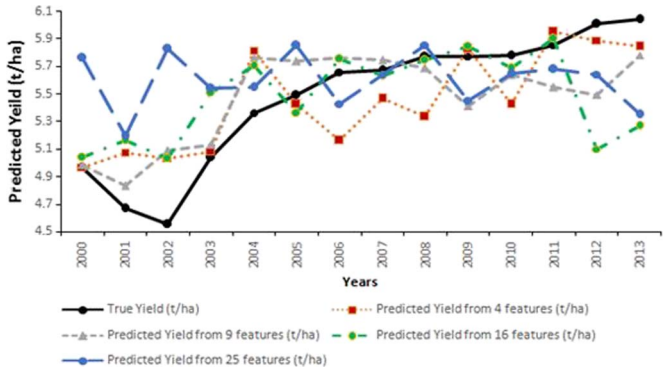

Fig. 5. Comparative analysis of the predicted yield versus the true yield for every year (2000 to 2013) using different numbers of features.

Model validation is one of the most important works in remote sensing data analysis. A common method to validate models is to plot the measured values against the predicted values, and the correlation coefficient is used to validate the final results. However, this method is inadequate to evaluate the performance of mechanistic models [72]. In this paper, we not only used the traditional validation method considering the correlation coefficient (R) [73], in conjunction with root-mean-squared error (rmse) [73], but also used other metrics like the average relative error (RE) [75], [76], mean absolute error (MAE) [73], and mean biased error (MBE) [73] to compare the predicted results and observed results.

IV. Results and Discussions

The experiments of dividing the NDVI sample space into equal-sized blocks are carried with 2 by 2, 3 by 3, 4 by 4, and 5 by 5 equal-sized blocks which correspond to 4, 9, 16, and 25 features, respectively. No further division of the sample space is done because we observed that the accuracy of the SNN model in predicting the output crop yield decreased significantly on further divisions. On increasing the number of features beyond 16, our model overfits the data and learns the noise in the data, thus decreasing the accuracy significantly. The experimental results for all of the experiments and their corresponding relative errors (%) between the predicted and true crop yields are provided in Table II.

From the table, we can see that the relative error between the predicted yield and the true yield reached as low as 0.13%, which proves the accuracy of our methodology. However, in some cases, particularly for 2002, we can see that the relative error is between 10.42% and 27.97%, which is poor when compared to other years. This is due to the fact that the NDVI for the middle ten days of March was missing from the USGS database as said earlier (see Section II), and we used linear interpolation technique to approximate the NDVI values for these missing days. The interpolation technique was not able to truly approximate the missing values, so it was reflected in the results. A graphical analysis of the predicted and true yields for different numbers of features for all of the years from 2000 to 2013 shows that the predicted yield curve from the nine-feature model best represents the true yield curve (see Fig. 5).

TABLE II
PREDICTED YIELD SIX WEEKS BEFORE HARVEST USING DIFFERENT NUMBERS OF FEATURES AND THEIR RELATIVE ERROR IN PERCENT COMPARED TO THE ACTUAL YIELD DURING HARVEST BASED ON LEAVE-ONE-OUT CROSS-VALIDATION TECHNIQUE

Year	True Yield (t/ha)	4 Features Model		9 Features Model		16 Features Model		25 Features Model	
		Predicted Yield (t/ha)	Relative Error (%)	Predicted Yield (t/ha)	Relative Error (%)	Predicted Yield (t/ha)	Relative Error (%)	Predicted Yield (t/ha)	Relative Error (%)
2000	4.96	4.96	0.13	4.98	0.44	5.03	1.48	5.76	16.10
2001	4.66	5.07	8.72	4.83	3.56	5.16	10.56	5.19	11.24
2002	4.55	5.02	10.42	5.08	11.76	5.03	10.47	5.82	27.97
2003	5.04	5.08	0.89	5.13	1.84	5.50	9.26	5.53	9.87
2004	5.36	5.81	8.44	5.76	7.51	5.70	6.33	5.55	3.48
2005	5.49	5.42	-1.24	5.73	4.46	5.35	-2.42	5.85	6.59
2006	5.66	5.16	-8.76	5.76	1.87	5.75	1.66	5.42	-4.07
2007	5.67	5.46	-3.63	5.74	1.37	5.63	-0.65	5.64	-0.46
2008	5.77	5.33	-7.55	5.68	-1.44	5.74	-0.42	5.85	1.49
2009	5.77	5.83	0.97	5.41	-6.24	5.84	1.22	5.45	-5.55
2010	5.77	5.42	-6.16	5.64	-2.40	5.68	-1.61	5.64	-2.27
2011	5.85	5.94	1.62	5.54	-5.21	5.90	0.78	5.67	-2.99
2012	6.01	5.88	-2.02	5.49	-8.60	5.10	-15.13	5.64	-6.12
2013	6.04	5.84	-3.26	5.78	-4.25	5.26	-12.77	5.34	-11.44

TABLE III
COMPARATIVE EXPERIMENTAL RESULTS FOR CROP YIELD ESTIMATION WITH DIFFERENT NUMBERS OF FEATURES

No. of Features	R	Average Prediction accuracy (%)	RE (%)	RMSE (t/ha)	MAE (t/ha)	MBE (t/ha)
4	0.77	95.43	4.56	0.30	0.24	-0.0245
9	0.80	95.64	4.35	0.28	0.23	-0.0009
16	0.52	94.65	5.34	0.41	0.28	0.0065
25	0.01	92.16	7.83	0.51	0.40	0.1276

TABLE IV
COMPARATIVE EXPERIMENTAL RESULTS FOR DIFFERENT MODELING METHODS WHEN APPLIED TO CROP YIELD PREDICTION WITH NINE FEATURES

Method	R	RMSE	MAE
Linear Regression	0.67	0.36	0.29
KNN	0.56	0.45	0.45
SVR	0.67	0.35	0.30
SNN(NeuCube)	0.81	0.29	0.24

We performed a comparative analysis of all of the models, i.e., 4, 9, 16, and 25 features on the basis of the performance metrics used. We noticed that the nine-feature model provided the best results for all of the performance evaluation parameters (see Table III). It showed a correlation coefficient of 0.81 along with an average prediction accuracy of 95.64%. Average prediction accuracy $= 100 - \text{RE}\,(\%)$. This model was followed by the 4-feature and 16-feature models with average prediction accuracies of 95.49% and 94.67%, respectively, while the 25-feature model showed the worst performance with a prediction accuracy of 92.17. The mean average errors (MAEs) were very small in all of the cases, with 0.29 t/ha being the lowest in the case of the nine-feature model and 0.41 being the worst in the case of the 25-feature model.

We have also tested the performance of the NeuCube in prediction by comparing it with other popular machine learning approaches such as the support vector regression (SVR), the linear regression technique, and the K-nearest neighbor algorithm (KNN). These algorithms were implemented in WEKA 3.6.11 (Waikato Environment for Knowledge Analysis) software which is a popular suite of machine learning software written in Java, developed at the University of Waikato, New Zealand [74]. All of the algorithms were tested with the nine-feature model, and they showed low correlation coefficients between the predicted and true yields ranging from 0.56 in case of the KNN algorithm to 0.67 in the case of linear regression and SVR (see Table IV). In comparison, NeuCube was able to produce a correlation coefficient of 0.81 (see Table IV) between the predicted yield and the true yield.

Linear regression was implemented by the ridge regression method [80], where the value of the ridge parameter was $1.0 * 10^{-8}$. In KNN, k, which represents the number of nearest neighbors, was fixed to 1. SVR was implemented using polynomial kernel functions with an epsilon parameter of $1.0 * 10^{-12}$ and a default complexity constant of 1. All of the models, i.e., linear regression, KNN, and SVR, use cross-validation technique for training and testing of the model.

Tables V and VI report the experimental results obtained by the threefold and fivefold cross-validation techniques, respectively. By analyzing the tables, we can see that the accuracies obtained are similar to those achieved by the leave-one-out cross-validation technique.

The middle ten days of April were the critical growth stage of the winter wheat in our study region as concluded by previous studies also [1]. The growth condition of winter wheat in this period might contain more yield information than other periods at all growth stages. Taking into consideration the method of yield prediction presented in this paper, the results could depend on the relationship between spatial accumulated NDVI and final production until the middle ten days of April to accurately predict winter wheat production. Consulting the phenoloy calendar of winter wheat in this region, we observed that winter wheat from the middle ten days of April was at the growth stage between booting and heading, which is the middle of all of the growth stages. At the middle stage, vegetative

TABLE V
PREDICTED YIELD SIX WEEKS BEFORE HARVEST USING DIFFERENT NUMBERS OF FEATURES AND THEIR RELATIVE ERROR IN PERCENT COMPARED TO THE ACTUAL YIELD DURING HARVEST BASED ON THREEFOLD CROSS-VALIDATION TECHNIQUE

Year	True Yield (t/ha)	4 Features Model		9 Features Model		16 Features Model		25 Features Model	
		Predicted Yield (t/ha)	Relative Error (%)	Predicted Yield (t/ha)	Relative Error (%)	Predicted Yield (t/ha)	Relative Error (%)	Predicted Yield (t/ha)	Relative Error (%)
2000	4.96	5.07	2.22	5.01	1.01	5.25	5.85	5.72	15.36
2001	4.66	4.95	6.22	4.85	4.08	5.42	16.31	5.76	23.54
2002	4.55	5.72	25.69	5.12	12.53	5.34	17.36	5.34	17.37
2003	5.04	5.29	4.96	5.21	3.44	5.74	13.84	5.64	11.93
2004	5.36	5.76	7.46	5.68	5.88	5.85	9.22	5.25	-2.15
2005	5.49	5.06	-7.89	5.40	-1.60	5.38	-2.04	5.34	-2.77
2006	5.66	5.22	-7.86	5.38	-4.87	5.44	-3.91	5.77	1.90
2007	5.67	5.54	-2.29	5.34	-5.90	5.16	-8.93	5.33	-6.04
2008	5.77	5.63	-2.43	5.76	-0.17	5.52	-4.34	5.52	-4.36
2009	5.77	5.72	-0.87	5.57	-3.52	5.62	-2.62	4.72	-18.26
2010	5.77	5.88	1.92	5.79	0.35	5.55	-3.76	5.45	-5.57
2011	5.85	5.95	1.71	5.61	-4.18	5.66	-3.21	5.65	-3.47
2012	6.01	5.95	-1.00	5.99	-0.33	5.30	-11.88	5.61	-6.73
2013	6.04	5.82	-3.64	5.95	-1.49	5.67	-6.13	5.53	-8.44

TABLE VI
PREDICTED YIELD SIX WEEKS BEFORE HARVEST USING DIFFERENT NUMBERS OF FEATURES AND THEIR RELATIVE ERROR IN PERCENT COMPARED TO THE ACTUAL YIELD DURING HARVEST BASED ON FIVEFOLD CROSS-VALIDATION TECHNIQUE

Year	True Yield (t/ha)	4 Features Model		9 Features Model		16 Features Model		25 Features Model	
		Predicted Yield (t/ha)	Relative Error (%)	Predicted Yield (t/ha)	Relative Error (%)	Predicted Yield (t/ha)	Relative Error (%)	Predicted Yield (t/ha)	Relative Error (%)
2000	4.96	5.41	9.01	5.04	1.63	5.21	5.04	5.16	4.12
2001	4.66	5.02	7.73	5.05	8.37	5.49	17.91	5.51	18.15
2002	4.55	5.36	17.88	5.06	11.21	5.59	22.86	5.53	21.56
2003	5.04	5.06	0.34	5.07	0.60	5.62	11.48	5.68	12.73
2004	5.36	5.77	7.70	5.18	-3.36	5.34	-0.45	5.49	2.46
2005	5.49	5.37	-2.28	5.64	2.69	5.84	6.41	5.37	-2.25
2006	5.66	5.50	-2.89	5.65	-0.18	5.68	0.37	5.33	-5.75
2007	5.67	5.50	-3.03	5.31	-6.32	5.61	-1.08	5.41	-4.61
2008	5.77	5.38	-6.75	5.74	-0.57	5.76	-0.16	5.40	-6.35
2009	5.77	5.53	-4.08	5.24	-9.19	5.12	-11.24	5.61	-2.69
2010	5.77	5.64	-2.18	5.77	0.07	5.54	-3.91	5.56	-3.58
2011	5.85	5.34	-8.74	5.54	-5.25	5.85	-0.02	5.38	-8.12
2012	6.01	5.67	-5.64	5.68	-5.53	5.68	-5.52	5.65	-6.04
2013	6.04	5.88	-2.65	5.96	-1.32	5.74	-4.97	5.63	-6.79

growth and reproductive growth were coinstantaneous, and florets, pistils, stamens, and pollen grains developed gradually. The numbers of floret and panicle grain were mainly decided by the growth status at this stage. Thus, the nutrition accumulation and growth status were critical to the final reproductive growth and yield of winter wheat. First, we used the ten-day NDVI values for just the middle ten days of April. However, no acceptable or reasonable results were observed from the direct correlation analysis. Moreover, a higher correlation coefficient was obtained with the NDVI integrated over several periods. The reason is that some periods are more important for crop yield, such as the heading to flowering stages for winter wheat.

V. DISCUSSIONS AND CONCLUSION

In this paper, we have presented an SNN model to make timely prediction of crop yield. The model is using spatial accumulation of blocks of MODIS-NDVI 250-m resolution data and historical crop yield data. The proposed model is introducing for the first time SNNs as promising techniques in remote

sensing, in our case here—for spatiotemporal data modeling, analysis, and land use/crop prediction. This study demonstrated that it is possible to develop a successful yield estimation model using the proposed SNN technique. The SNN performed much better than the other traditional approaches. The stability and accuracy of the SNN yield estimation model result from several important characteristics of the model: 1) capabilities of SNN to capture spatiotemporal patterns from spatiotemporal data through the application of time-dependent machine learning rules; 2) SNN model interpretability for the understanding of the data and the processes that generated them; 3) integrated use of remotely sensed data together with historical statistical information, parameters retrieved from satellite images were coalesced by the main growing season of the crop; and 4) precise division of the study area based on agricultural knowledge and careful selection of sample data.

From the experimental analysis, we have concluded that the accuracy in the prediction of the crop yield with the MODIS-NDVI was satisfactory. We only used the NDVI from the first week of March to the middle ten days of April to predict winter wheat yields, while its ripe time was the first ten days of June. We were able to make a good prediction of the winter wheat yield about 40 days ahead of harvest time, i.e., the prediction could be made at the booting–heading stage of winter wheat, which was significant to the winter wheat yield in this region. The NDVI images were collected for every year during the same duration from beginning of March to the middle of April. The images are ten-day composite data at an interval of every five days. We can use the variation in the pixel values of the NDVI images during the same timeframe between the subsequent years and the statistical interannual variation of wheat yield to train the SNN model. This model can then predict the interannual variation of crop yield. This is a possible future direction of this work. In practical situations, there are many types of crops growing together in a small region. However, the crop yield is only related to the NDVI data extracted from the corresponding crop planting areas. Therefore, identification of the crop planting area is another crucial part of the estimation model development and implementation.

We intend to extend these first results to the development of a large-scale NeuCube-based system for remote sensing data analysis and event prediction to become available for research and commercial use. A generic and preliminary version of NeuCube is now available free from http://www.kedri.aut.ac.nz/neucube/. The proposed SNN models are scalable in terms of dimensionality of the SNNc that can map with a high-precision large-scale and large-dimensionality satellite image data. As a NeuCube simulator is available in PyNN, along with Java and MATLAB [37], this makes it possible for a direct implementation of such models on all available neuromorphic hardware platforms (e.g., [77]–[79]) for very fast processing of large volumes of data in an online real-time mode. Computational platforms such as the Manchester SpiNNaker [77] and the IBM TrueNorth [78], along with hybrid neuromorphic chips [79] of thousands and millions of spiking neurons with very low energy consumption can now be used for satellite image data. In this respect, the proposed method is the first to enable a direct use of neuromorphic hardware for such data modeling and analysis.

REFERENCES

[1] J. Huang, H. Wang, Q. Dai, and D. Han, "Analysis of NDVI data for crop identification and yield estimation," in *IEEE J. Sel. Topics Appl. Earth Observ. Remote Sens.*, vol. 7, no. 11, pp. 4374–4384, Nov. 2014.

[2] P. C. Doraiswamy, S. Moulin, P. W. Cook, and A. Stern, "Crop yield assessment from remote sensing," *Photogramm. Eng. Remote Sens.*, vol. 69, pp. 665–674, Jun. 2003.

[3] K. N. Chaudhari, R. Tripathy, and N. K. Patel, "Spatial wheat yield prediction using crop simulation model, GIS, remote sensing and ground observed data," *J. Agrometeorol.*, vol. 12, pp. 174–180, Dec. 2010.

[4] V. K. Boken and C. F. Shaykewich, "Improving an operational wheat yield model using phenological phase-based normalized difference vegetation index," *Int. J. Remote Sens.*, vol. 23, pp. 4155–4168, Sep. 2002.

[5] M. S. Mkhabela, P. Bullock, S. Raj, S. Wang, and Y. Yang, "Crop yield forecasting on the Canadian Prairies using MODIS NDVI data," *Agricultural Forest Meteorol.*, vol. 151, pp. 385–393, Mar. 2011.

[6] T. Lillesand, R. W. Kiefer, and J. Chipman, *Remote Sensing and Image Interpretation*, 2nd ed. Hoboken, NJ, USA: Wiley, 2008.

[7] K. Soudani *et al.*, "Ground-based network of NDVI measurements for tracking temporal dynamics of canopy structure and vegetation phenology in different biomes," *Remote Sens. Environ.*, vol. 123, pp. 234–245, Aug. 2012.

[8] F. Maselli and F. Rembold, "Analysis of GAC NDVI data for cropland identification and yield forecasting in Mediterranean African countries," *Photogramm. Eng. Remote Sens.*, vol. 67, pp. 593–602, May 2001.

[9] M. S. Mkhabela, M. S. Mkhabelab, and N. N. Mashininic, "Early maize yield forecasting in the four agro-ecological regions of Swaziland using NDVI data derived from NOAA's-AVHRR," *Agricultural Forest Meteorol.*, vol. 129, pp. 1–9, Mar. 2005.

[10] R. Balaghi, B. Tychon, H. Eerens, and M. Jlibene, "Empirical regression models using NDVI, rainfall and temperature data for the early prediction of wheat grain yields in Morocco," *Int. J. Appl. Earth Observ. Geoinf.*, vol. 10, no. 4, pp. 438–452, Dec. 2008.

[11] R. Benedetti and P. Rossini, "On the use of NDVI profiles as a tool for agricultural statistics: The case study of wheat yield estimate and forest in Emilia Romagma," *Remote Sens. Environ.*, vol. 45, pp. 311–326, Sep. 1993.

[12] M. S. Rasmussen, "Operational yield forecast using AVHRR NDVI data: Reduction of environmental and inter-annual variability," *Int. J. Remote Sens.*, vol. 18, pp. 1059–1077, Mar. 1997.

[13] J. E. Lewis, J. Rowland, and A. Nadeau, "Estimating maize production in Kenya using NDVI: Some statistical considerations," *Int. J. Remote Sens.*, vol. 19, no. 13, pp. 2609–2617, Sep. 1998.

[14] C. J. Tucker *et al.*, "An extended AVHRR 8-km NDVI dataset compatible with MODIS and SPOT vegetation NDVI data," *Int. J. Remote Sens.*, *Remote Sens.*, vol. 26, no. 20, pp. 4485–4498, Oct. 2005.

[15] A. A. Gitelson and Y. J. Kaufman, "MODIS NDVI optimization to fit the AVHRR data series—Spectral considerations," *Remote Sens. Environ.*, vol. 66, pp. 343–350, Dec. 1998.

[16] J. Q. Ren, Z. X. Chen, Q. B. Zhou, and H. J. Tang, "Regional yield estimation for winter wheat with MODIS-NDVI data in Shandong, China," *Int. J. Appl. Earth Observ.*, vol. 10, no. 4, pp. 403–413, Dec. 2008.

[17] I. Becker-Reshef, E. Vermote, M. Lindeman, and C. Justice, "A generalized regression-based model for forecasting winter wheat yields in Kansas and Ukraine using MODIS data," *Remote Sens. Environ.*, vol. 114, pp. 1312–1323, Jun. 2010.

[18] B. Mulianga, A. Begue, M. Simoes, and P. Todoroff, "Forecasting regional sugarcane yield based on time integral and spatial aggregation of MODIS NDVI," *Remote Sens.*, vol. 5, pp. 2184–2199, May 2013.

[19] Y. Shao, J. B. Campbell, G. N. Taff, and B. Zheng, "An analysis of cropland mask choice and ancillary data for annual corn yield forecasting using MODIS data," *Int. J. Appl. Earth Observ.*, vol. 38, pp. 78–87, Jun. 2015.

[20] J. C. Taylor, G. A. Wood, and G. Thomas, "Mapping yield potential with remote sensing," presented at the First European Conference on Precision Agriculture, Warwick University Conference Centre, Oxford, U.K., Sep. 1997.

[21] S. GopalaPillai and L. Tian, "In-field variability detection and spatial yield modeling for corn using digital aerial imaging," *Trans. Amer. Soc. Agricultural Eng.*, vol. 42, no. 6, pp. 1911–1920, Nov. 1999.

[22] G. B. Senay, A. D. Ward, J. G. Lyon, N. R. Fausey, and S. E. Nokes, "Manipulation of high spatial resolution aircraft remote sensing data for use in site-specific farming," *Trans. Amer. Soc. Agricultural Eng.*, vol. 41, no. 2, pp. 489–495, Apr. 1998.

[23] C. A. Black, *Soil Fertility Evaluation and Control*. Boca Raton, FL, USA: CRC Press, 1993, pp. 92–103.

[24] S. Haykin, *Neural Networks—A Comprehensive Foundation*, 2nd ed. Upper Saddle River, NJ, USA: Prentice-Hall, 1999, pp. 156–255.

[25] G. Zhang, B. Eddy Patuwo, and M. Y. Hu, "Forecasting with artificial neural networks: The state of the art," *Int. J. Forecast.*, vol. 14, no. 1, pp. 35–62, Mar. 1998.

[26] Z. Xin and B. A. Engel, "Classification of multispectral remote sensing data using neural networks vs statistical methods," *Amer. Soc. Agricultural Eng.*, vol. 90-7552, p. 10, 1990.

[27] D. Ranaweera, "Application of radial basis function neural network model for short-term load forecasting," *Proc. Inst. Elect. Eng.—Gener. Transmiss. Distrib.*, vol. 142, no. 1, p. 45, Jan. 1995.

[28] A. Hodgkin and A. Huxley, "A quantitative description of membrane current and its application to conduction and excitation in nerve," *J. Physiol.*, vol. 117, no. 4, pp. 500–544, Aug. 1952.

[29] W. Gerstner, "Time structure of the activity in neural network models," *Phys. Rev. E, Stat. Phys. Plasmas Fluids Relat. Interdiscip. Top.*, vol. 51, no. 1, pp. 738–758, Jan. 1995.

[30] W. Maass and A. Zador, "Computing and learning with dynamic synapses," *Pulsed Neural Netw.*, vol. 6, pp. 321–336, 1999.

[31] W. Gerstner and W. M. Kistler, *Spiking Neuron Models: Single Neurons, Populations, Plasticity*. Cambridge, MA, USA: Cambridge Univ. Press, 2002.

[32] E. Izhikevich, "Which model to use for cortical spiking neurons?" *IEEE Trans. Neural Netw.*, vol. 15, no. 5, pp. 1063–1070, Sep. 2004.

[33] E. Izhikevich, "Polychronization: Computation with spikes," *Neural Comput.*, vol. 18, no. 2, pp. 245–282, Feb. 2006.

[34] A. Belatreche, L. P. Maguire, and M. McGinnity, "Advances in design and application of spiking neural networks," *Soft Comput.*, vol. 11, no. 3, pp. 239–248, Mar. 2006.

[35] R. Brette *et al.*, "Simulation of networks of spiking neurons: A review of tools and strategies," *J. Comput. Neurosci.*, vol. 23, no. 3, pp. 349–398, Dec. 2007.

[36] S. Thorpe and J. Gautrais, "Rank order coding," *Comput. Neurosci., Trends Res.*, vol. 13, pp. 113–119, 1998.

[37] N. Kasabov *et al.*, "Evolving spatio-temporal data machines based on the NeuCube neuromorphic framework: Design methodology and selected applications," *Neural Netw.*, vol. 78, pp. 1–14, Jun. 2016.

[38] N. Kasabov, *Evolving Connectionist Systems: The Knowledge Engineering Approach*. New York, NY, USA: Springer-Verlag, 2007.

[39] S. Wysoski, L. Benuskova, and N. Kasabov, "Evolving spiking neural networks for audiovisual information processing," *Neural Netw.*, vol. 23, no. 7, pp. 819–835, Sep. 2010.

[40] S. Schliebs and N. Kasabov, "Evolving spiking neural network—A survey," *Evolving Syst.*, vol. 4, no. 2, pp. 87–98, Jun. 2013.

[41] N. Kasabov, K. Dhoble, N. Nuntalid, and G. Indiveri, "Dynamic evolving spiking neural networks for on-line spatio- and spectro-temporal pattern recognition," *Neural Netw.*, vol. 41, pp. 188–201, May 2013.

[42] A. Mohemmed, S. Schliebs, S. Matsuda, and N. Kasabov, "Training spiking neural networks to associate spatio-temporal input–output spike patterns," *Neurocomputing*, vol. 107, pp. 3–10, May 2013, doi: 10.1016/j.neucom.2012.08.034.

[43] N. Kasabov, "Evolving, probabilistic spiking neural networks and neurogenetic systems for spatio- and spectro-temporal data modelling and pattern recognition," *INNS Mag. Natural Intell.*, vol. 1, no. 2, pp. 23–37, 2012.

[44] N. Kasabov, V. Feigin, Z. Hou, and Y. Chen, "Improved method and system for predicting outcomes based on spatio/spectro-temporal data," NZ Provisional Patent Appl. 614 708, Aug. 26, 2013.

[45] N. Kasabov, "NeuCube: A spiking neural network architecture for mapping, learning and understanding of spatio-temporal brain data," *Neural Netw.*, vol. 52, pp. 62–76, Apr. 2014.

[46] N. Kasabov *et al.*, "Evolving spiking neural networks for personalised modelling, classification and prediction of spatio-temporal patterns with a case study on stroke," *Neurocomputing*, vol. 134, pp. 269–279, Jun. 2014.

[47] Y. C. Shi and D. L. Jia, *Agricultural Atlas of the Huang-Huai-Hai Plain*. Beijing, China: Beijing Agricultural Univ. Press, 1988.

[48] A. A. Gitelson, Y. J. Kaufman, and M. N. Merzlyak, "An atmospherically resistant "green" vegetation index (ARGI) for EOS-MODIS," *Remote Sens. Environ.*, vol. 58, no. 3, pp. 289–298, Dec. 1997.

[49] A. R. Huete and H. Q. Liu, "An error and sensitivity analysis of the atmospheric and soil-correcting variants of the NDVI for the MODIS-EOS," *IEEE Trans. Geosci. Remote Sens.*, vol. 32, no. 4, pp. 897–905, Jul. 1994.

[50] A. R. Huete, C. Justice, and H. Q. Liu, "Development of vegetation and soil indices for MODIS-EOS," *Remote Sens. Environ.*, vol. 49, no. 3, pp. 224–234, Sep. 1994.

[51] A. R. Huete, H. Q. Liu, K. Batchily, and V. Leeuwen, "A comparison of vegetation indices over a global set of TM images for EOS-MODIS," *Remote Sens. Environ.*, vol. 59, no. 3, pp. 440–451, Mar. 1997.

[52] A. R. Huete, K. Didan, T. Miura, E. P. Rodriguez, X. Gao, and L. G. Ferreira, "Overview of the radiometric and biophysical performance of the MODIS vegetation indices," *Remote Sens. Environ.*, vol. 83, no. 1/2, pp. 195–213, Nov. 2002.

[53] Y. J. Kaufman and D. Tanré, "Strategy for direct and indirect methods for correcting the aerosol effect on remote sensing: From AVHRR to EOS-MODIS," *Remote Sens. Environ.*, vol. 55, no. 1, pp. 65–79, Jan. 1996.

[54] W. J. D. Van Leeuwen, A. R. Huete, and T. W. Laing, "MODIS vegetation index compositing approach: A prototype with AVHRR data," *Remote Sens. Environ.*, vol. 69, no. 3, pp. 264–280, Sep. 1999.

[55] X. Xiao *et al.*, "Mapping paddy rice agriculture in southern China using multi-temporal MODIS images," *Remote Sens. Environ.*, vol. 95, no. 4, pp. 480–492, Apr. 2005.

[56] P. S. A. Beck, C. Atzberger, K. A. Høgda, B. Johansen, and A. K. Skidmore, "Improved monitoring of vegetation dynamics at very high latitudes: A new method using MODIS NDVI," *Remote Sens. Environ.*, vol. 100, no. 3, pp. 321–334, Feb. 2006.

[57] B. D. Wardlow, S. L. Egbert, and J. H. Kastens, "Analysis of time-series MODIS 250 m vegetation index data for crop classification in the U.S. Central Great Plains," *Remote Sens. Environ.*, vol. 108, no. 3, pp. 290–310, Jun. 2007.

[58] R. S. Lunetta, J. F. Knight, J. Ediriwichrema, J. G. Lyon, and L. D. Worthy, "Land-cover change detection using multi-temporal MODIS NDVI data," *Remote Sens. Environ.*, vol. 105, no. 2, pp. 142–154, Nov. 2006.

[59] J. Kastens, T. Kastens, D. Kastens, K. Price, E. Martinko, and R. Lee, "Image masking for crop yield forecasting using AVHRR NDVI time series imagery," *Remote Sens. Environ.*, vol. 99, no. 3, pp. 341–356, Nov. 2005.

[60] N. Kasabov, "To spike or not to spike: A probabilistic spiking neuron model," *Neural Netw.*, vol. 23, no. 1, pp. 62–76, Jan. 2010.

[61] L. Lapicque, "Recherches quantitatives sur l'excitation électrique des nerfs traitée comme une polarisation," *J. Physiol. Pathol. Gen.*, vol. 9, no. 1, pp. 620–635, 1907.

[62] R. Stein, "Some models of neuronal variability," *Biophys. J.*, vol. 7, no. 1, pp. 37–68, Jan. 1967.

[63] F. Ponulak and A. Kasinski, "Introduction to spiking neural networks: Information processing, learning and applications," *Acta Neurobiologiae Experiment.*, vol. 71, no. 4, pp. 409–433, Dec. 2010.

[64] C. S. Sherrington, "The central nervous system," in *A Textbook of Physiology*, F. M. Macmillian Ed., 7th ed. London, U.K.: Macmillan, 1897, Part III, p. 929.

[65] M. Bennett, "The early history of the synapse: From Plato to Sherrington," *Brain Res. Bull.*, vol. 50, no. 2, pp. 95–118, Sep. 1999.

[66] E. R. Kandel, J. H. Schwartz, and T. M. Jessell, *Principles of Neural Science*, vol. 4. New York, NY, USA: McGraw-Hill, 2000, pp. 1227–1246.

[67] W. Maass, "Lower bounds for the computational power of networks of spiking neurons," *Neural Comput.*, vol. 8, no. 1, pp. 1–40, Jan. 1996.

[68] W. Gerstner and W. Kistler, "Mathematical formulations of Hebbian learning," *Biol. Cybern.*, vol. 87, no. 5/6, pp. 404–415, Dec. 2002.

[69] E. Chicca *et al.*, "A multichip pulse-based neuromorphic infrastructure and its application to a model of orientation selectivity," *IEEE Trans. Circuits Syst. I, Reg. Papers*, vol. 54, no. 5, pp. 981–993, May 2007.

[70] S. Song, K. D. Miller, and L. F. Abbott, "Competitive Hebbian learning through spike-timing-dependent synaptic plasticity," *Nature Neurosci.*, vol. 3, no. 9, pp. 919–926, Sep. 2000.

[71] R. Kohavi, "A study of cross-validation and bootstrap for accuracy estimation and model," in *Proc. IJCAI*, 1995, pp. 1137–1143.

[72] K. Kobayashi and M. Salam, "Comparing simulated and measured values using mean squared deviation and its components," *Agronomy J.*, vol. 92, no. 2, pp. 345–352, Apr. 2000.

[73] C. Willmott and K. Matsuura, "Advantages of the mean absolute error (MAE) over the root mean square error (rmse) in assessing average model performance," *Climate Res.*, vol. 30, pp. 79–82, 2005.

[74] I. H. Witten, H. Ian, and E. Frank, *Data Mining: Practical Machine Learning Tools and Techniques*. San Francisco, CA, USA: Morgan Kaufmann, 2005.

[75] E. W. Weisstein, "Relative Error," Wolfram Research, 2016. [Online]. Available: http://mathworld.wolfram.com/RelativeError.html. Accessed: Jul. 9, 2016.

[76] X. Rong and Z. Zhao, "Relative error measures for evaluation of estimation algorithms," in *Proc. IEEE 8th Int. Conf. Inf. Fus.*, Jul. 2005, vol. 1, pp. 1–8.

[77] S. B. Furber, F. Galluppi, S. Temple, and L. A. Plana, "The SpiNNaker Project," *Proc. IEEE*, vol. 102, no. 5, pp. 652–665, May 2014.

[78] P. A. Merolla *et al.*, "A million spiking neuron integrated circuit with a scalable communication network and interface," *Science*, vol. 345, no. 6197, pp. 668–673, Aug. 2014.
[79] G. Indiveri *et al.*, "Neuromorphic silicon neuron circuits," *Frontiers Neurosci.*, vol. 5, pp. 1–23, 2011.
[80] A. E. Hoerl and R. W. Kennard, "Ridge regression: Biased estimation for nonorthogonal problems," *Technometrics*, vol. 12, no. 1, pp. 55–67, Feb. 1970.

Pritam Bose was born in Kolkata, India, in 1991. He received the B.Tech. degree in electronics and communications engineering from the West Bengal University of Technology, West Bengal, India, in 2013 and the M.Sc. degree in telecommunications engineering from the University of Trento, Trento, Italy, in 2016.

His current research interests are in the areas of remote sensing, radar and SAR, signal processing, computer vision, and pattern recognition.

Nikola K. Kasabov (F'10) received the M.Sc. degree in electrical engineering, specializing in computer science, and the Ph.D. degree in mathematical sciences from the Technical University, Sofia, Bulgaria, in 1971 and 1975, respectively.

He is the Director of the Knowledge Engineering and Discovery Research Institute and Personal Chair of Knowledge Engineering with Auckland University of Technology, Auckland, New Zealand. He has published over 550 works in the areas of intelligent systems, neural networks, connectionist and hybrid connectionist systems, fuzzy systems, expert systems, bioinformatics, and neuroinformatics.

Dr. Kasabov is a Fellow of the Royal Society of New Zealand and a Distinguished Visiting Fellow of the RAE U.K. He is a Past President of the International Neural Network Society (INNS) and the Asia Pacific Neural Network Assembly (APNNA) and currently a member of the INNS and APNNA Governing Boards.

Lorenzo Bruzzone (S'95–M'98–SM'03–F'10) received the Laurea (M.S.) degree in electronic engineering (*summa cum laude*) and the Ph.D. degree in telecommunications from the University of Genoa, Genova, Italy, in 1993 and 1998, respectively.

He is currently a Full Professor of telecommunications with the University of Trento, Trento, Italy, where he teaches remote sensing, radar, pattern recognition, and electrical communications. He is the Founder and the Director of the Remote Sensing Laboratory, Department of Information Engineering and Computer Science, University of Trento. His current research interests are in the areas of remote sensing, radar and SAR, signal processing, and pattern recognition. He promotes and supervises research on these topics within the frameworks of many national and international projects. Among the others, he is the Principal Investigator of the *Radar for icy Moon exploration (RIME)* instrument in the framework of the *JUpiter ICy moons Explorer (JUICE)* mission of the European Space Agency. He is the author (or coauthor) of 161 scientific publications in referred international journals (111 in IEEE journals), more than 220 papers in conference proceedings, and 17 book chapters. He is the editor/coeditor of 16 books/conference proceedings and 1 scientific book. His papers are highly cited, as proven by the total number of citations (more than 15300) and the value of the h-index (63; source: Google Scholar).

Dr. Bruzzone ranked First Place in the Student Prize Paper Competition of the 1998 IEEE International Geoscience and Remote Sensing Symposium (Seattle, July 1998). Since that time, he has been the recipient of many international and national honors and awards. He was a Guest Coeditor of different special issues of international journals. He is the Cofounder of the IEEE International Workshop on the Analysis of Multi-Temporal Remote-Sensing Images (MultiTemp) series and is currently a member of the Permanent Steering Committee of this series of workshops. Since 2003, he has been the Chair of the SPIE Conference on Image and Signal Processing for Remote Sensing. Since 2013, he has been the founder Editor-in-Chief of the IEEE GEOSCIENCE AND REMOTE SENSING MAGAZINE. He is currently an Associate Editor of the IEEE TRANSACTIONS ON GEOSCIENCE AND REMOTE SENSING and the *Canadian Journal of Remote Sensing*. Since 2012, he has been appointed as a *Distinguished Speaker* of the IEEE Geoscience and Remote Sensing Society. He was invited as keynote speaker in 30 international conferences and workshops. Since 2009, he has been a member of the Administrative Committee of the IEEE Geoscience and Remote Sensing Society.

Reggio N. Hartono received the Bachelor's degree in information technology from the Swiss German University, BSD City, Java, Indonesia in 2008 and, after some time working in the industry, the Master's degree in computer science from the University of Indonesia, Depok, Indonesia, in 2011. He is currently working toward the Ph.D. degree in the Knowledge Engineering and Discovery Research Institute, Auckland University of Technology, Auckland, New Zealand.

His research revolves around adaptive methods for stream spatiotemporal data mining and its applications in geoscience and ecological modeling.